Electronic Supplementary Material (ESI) for Journal of Materials Chemistry A.

Supporting Information

Strongly Coupled Polypyrrole/Molybdenum Oxide Hybrid Films via Electrochemical Layer–by–Layer Assembly for Pseudocapacitors

Ming–Yue Zhang, Yu Song, Di Guo, Duo Yang, Xiaoqi Sun and Xiao–Xia Liu**

Department of Chemistry, Northeastern University, Shenyang 110819, China

E-mail: songyu@mail.neu.edu.cn; xxliu@mail.neu.edu.cn

1. CALCULATION METHODS

Specific capacitance calculation: Specific capacitances of different samples according to the constant current charge–discharge profiles are calculated from equation S1:

$$C = \frac{It}{m\Delta U} \quad \text{(S1)}$$

where C stands for specific capacitance (F g^{-1}), I is the discharge current (mA), t is the discharge time (s), m is the mass loading of the active materials (mg) and ΔU the potential window (V).

Specific capacitances of the ASC device from the constant current charge–discharge profiles are calculated from equation S2:

$$C = \frac{It}{mU} \quad \text{(S2)}$$

where C is the specific capacitance of the ASC (F g^{-1}), m is the mass of both electrodes (mg) and U is the potential window of the ACS (V).

Energy density and power density calculations for the ASC: Energy density (E, in Wh kg^{-1}) and power density (P, in W kg^{-1}) are calculated according to the equation S3 and S4:

$$E = \frac{1000}{2 \times 3600} CU^2 \quad \text{(S3)}$$

$$P = \frac{3600 \times E}{t} \quad \text{(S4)}$$

where C is the specific capacitance (F g^{-1}), U is the potential window (V) and t is the discharge time (s) in constant current charge/discharge profiles.

Capacitive and diffusion–controlled capacitance calculations: Specific capacitances were calculated based on CV curves at different scan rates according to the following equation S5:

$$C = \frac{S}{2 \times \Delta U \times v} \quad \text{(S5)}$$

where C stands for the specific capacitance (F g^{-1}), ΔU is the potential window (V), v is the scan rate (V s^{-1}), S is the integral area of the CV curve (A V g^{-1}).

Plotting C^{-1} vs. $v^{1/2}$ gives a linear relationship, assuming semi–infinite diffusion of ions, which can be described in the equation S6:

$$C^{-1} = \text{constant} \times v^{1/2} + C_T{}^{-1} \quad \text{(S6)}$$

where C, v and C_T are specific capacitance calculated from the corresponding CV curve, scan rate and total capacitance, respectively. Data points collected at larger scan rates deviated from this linear correlation because of the deviation from semi–infinite ion diffusion. Masking the deviated data points, fitting the others and extrapolating the fitting line to y–axis can give $C_T{}^{-1}$. C_T represents the highest possible capacitance because ions can react adequately with active material in enough time. C_T is the sum of C_C and C_D. C_C and C_D represent capacitive and diffusion–controlled capacitance, respectively.

Similarly, a linear correlation in C vs $v^{-1/2}$ plot can also be obtained. Fitting the data points at slow scan rates and extrapolating the fitting line to y–axis can yield C_C, since C_D with slow kinetic can be negligible when reaction time tends to infinitesimal. Subtracting C_C from C_T yields C_D. C_T, C_C and C_D are calculated to be 413.22 F g^{-1}, 303.17 F g^{-1} and 110.05 F g^{-1}, respectively.

EIS analysis method: The impedance of the electrode material can be described in equation S7:

$$Z(\omega) = \frac{1}{j\omega \times C(\omega)} \quad \text{(S7)}$$

where ω is pulsation [$\omega = 2\pi f$, f is the frequency (Hz)], $C(\omega)$ presents the capacitance as a function of the pulsation ω.

The impedance $Z(\omega)$ can be written in S8:

$$Z(\omega) = Z'(\omega) + jZ''(\omega) \quad \text{(S8)}$$

S7 and S8 lead to S9:

$$C(\omega)=\frac{1}{\omega\times[jZ'(\omega)-Z''(\omega)]}=\frac{-[Z''(\omega)+jZ'(\omega)]}{\omega|Z(\omega)|^2} \quad \text{(S9)}$$

The capacitance $C(\omega)$ can be written in S10:

$$C(\omega)=C'(\omega)-jC''(\omega) \quad \text{(S10)}$$

leading to S11 and S12:

$$C'(\omega)=\frac{-Z''(\omega)}{\omega|Z(\omega)|^2} \quad \text{(S11)}$$

$$C''(\omega)=\frac{Z'(\omega)}{\omega|Z(\omega)|^2} \quad \text{(S12)}$$

where $C'(\omega)$ and $C''(\omega)$ are the real part and imaginary part (ohm) of the capacitance $C(\omega)$.

The mass of PPy and MoO_x in the composite film: The LbL–PPy/MoO_x electrode was first immersed in 50 mL 2 M KOH solution for 24 h to dissolve the MoO_x materials. And then, the electrode was transferred in 100 mL deionized water for 12 h and washed to remove the residues. This electrode was further dried in vacuum oven at 60 °C for 10 h. The weight difference of the electrode is the mass of MoO_x (0.64 mg cm^{-2}). The active mass of LbL–PPy/MoO_x is ~1 mg cm^{-2}, therefore, the mass of PPy in the composite is ~0.36 mg cm^{-2}. We further verified the result using the XPS data. The mass percentage of N and Mo in the composite is ~ 7.1 % and 5.8 %. Based on their molecular weight, we can estimate that the mass ratio of PPy/MoO_x in the composite is ~0.52, which is agreed with the former experimental results.

Charge balance for cathode and anode: To maximize the performance of a pseudocapacitor, the charge (Q) stored in anode and cathode should be balanced, i.e. $Q_+ = Q_-$. The charge stored by each electrode depends on the specific capacitance (C_s), potential window (ΔU) and the mass of the active materials (m), following equation S13:

$$Q = C_S \times \Delta U \times m \qquad (S13)$$

In order to get $Q_+ = Q_-$ at 1 A g^{-1}, the mass ratio of the anode and cathode should follow Equation S14:

$$\frac{m_+}{m_-} = \frac{(C_{S,-}) \times (\Delta U_-)}{(C_{S,+}) \times (\Delta U_+)} = \frac{398 \times 1.2}{346 \times 1} = 1.38 \qquad (S14)$$

Where $C_{s,-}$=398 F g^{-1} with a potential window of 1.2 V and $C_{s,+}$=346 F g^{-1} with a potential window of 1 V. The calculated mass ratio between cathode and anode electrode is about 1.38.

2. SUPPLEMENTARY FIGURES

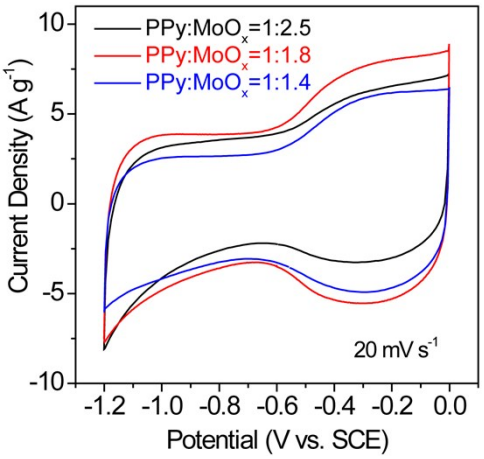

Figure S1. CV curves of LbL–PPy/MoO_x films with PPy:MoO_x ratio of 1:2.5, 1:1.8 and 1:1.4, respectively.

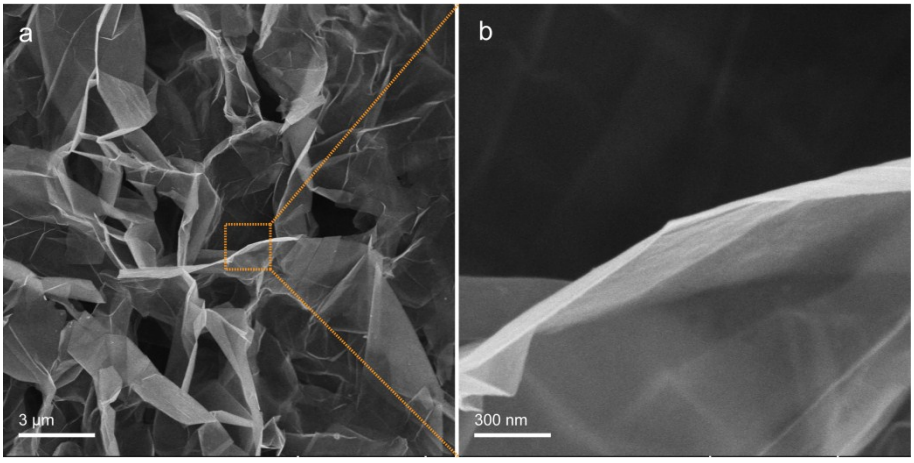

Figure S2. SEM image of films on a 3D electrochemically exfoliated graphite current collector (EG).

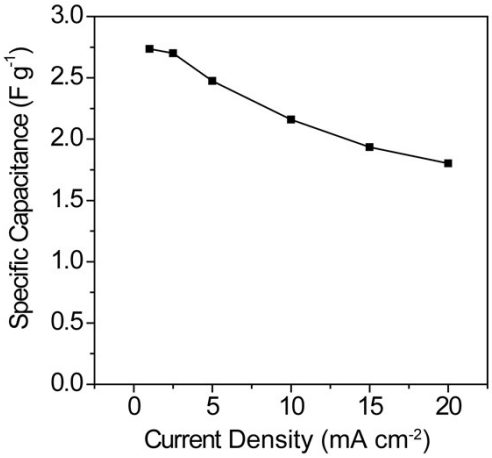

Figure S3. The specific capacitance of EG (current collector) as a function of current density.

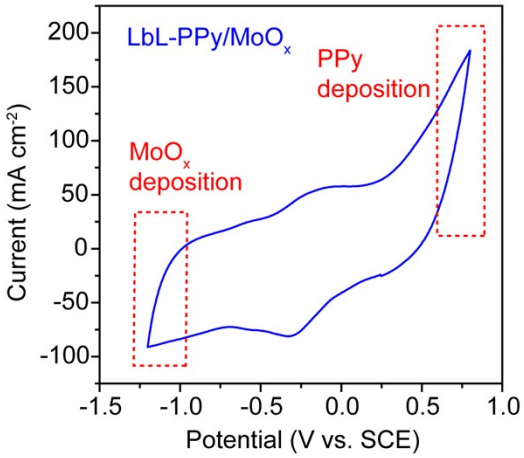

Figure S4. One cycle of CV curve of the electrochemical deposition process of LbL–PPy/MoO_x.

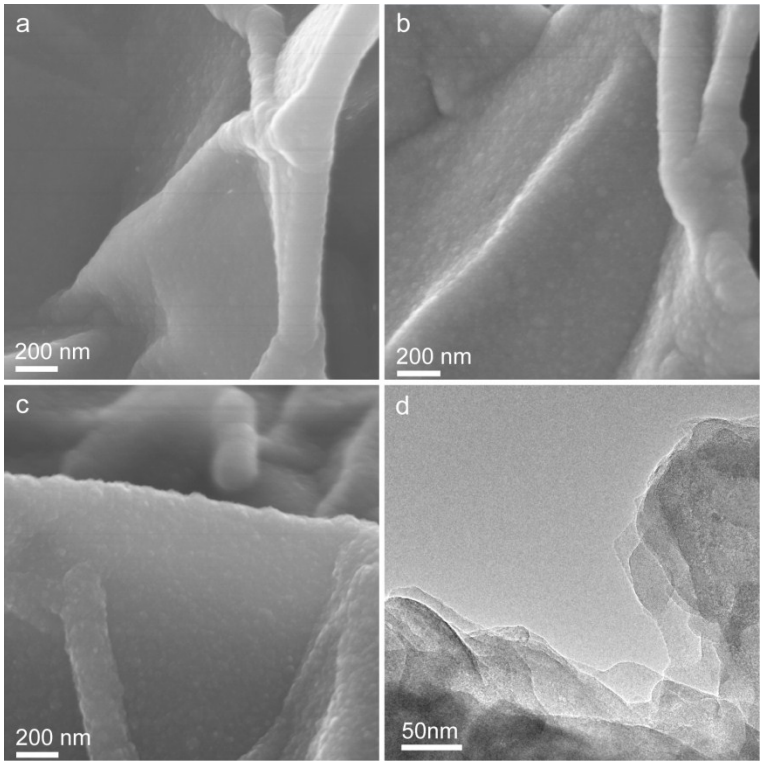

Figure S5. SEM images of (a) PPy, (b) MoO_x and (c) LbL–PPy/MoO_x. (d) TEM image of LbL structure of PPy/MoO_x.

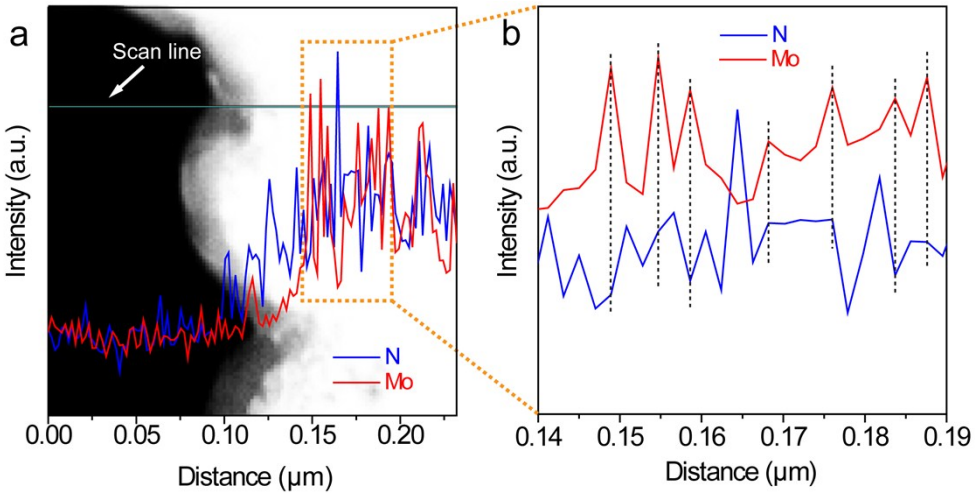

Figure S6. (a) The TEM linear EDX elemental scan of LbL–PPy/MoO_x. (b) The magnified signals at the selected area in (a).

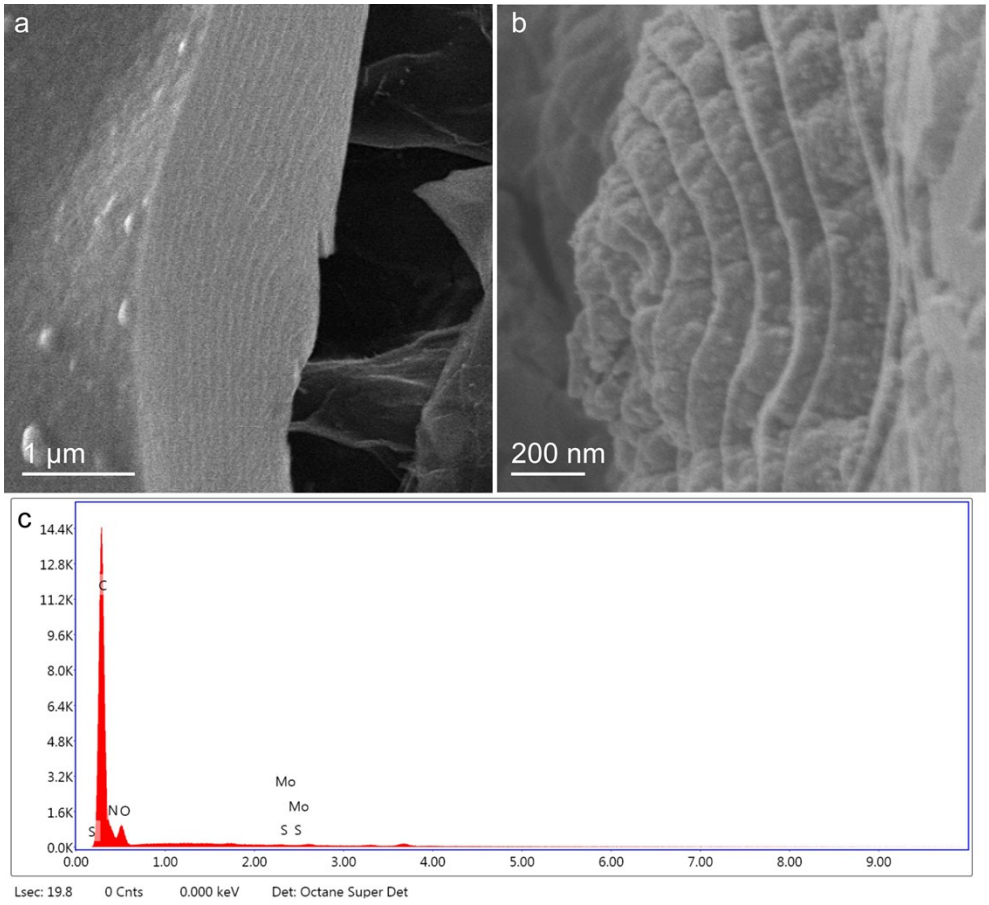

Figure S7. SEM images of (a) the as–prepared T–LbL–PPy/MoO_x sample and (b) the sample after KOH etching. (c) EDS spectra collected for the sample after KOH etching, indicating MoO_x was successfully removed.

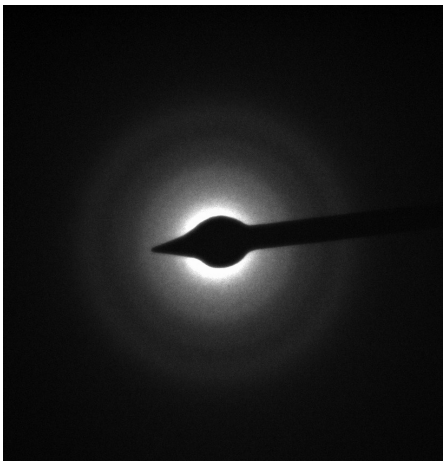

Figure S8 Selected area electron diffraction (SAED) pattern of LbL–PPy/MoO_x film. The diffusive rings indicate the amorphous nature of the material.

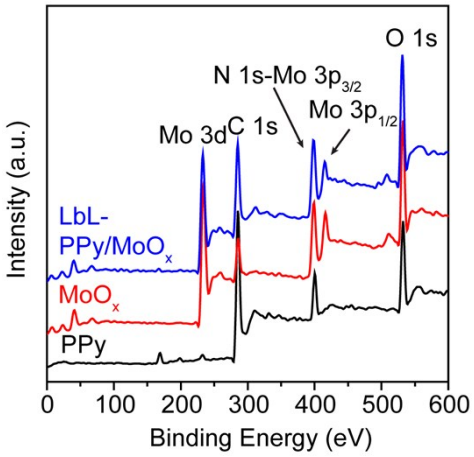

Figure S9. XPS survey spectrum of PPy, MoO_x and LbL–PPy/MoO_x.

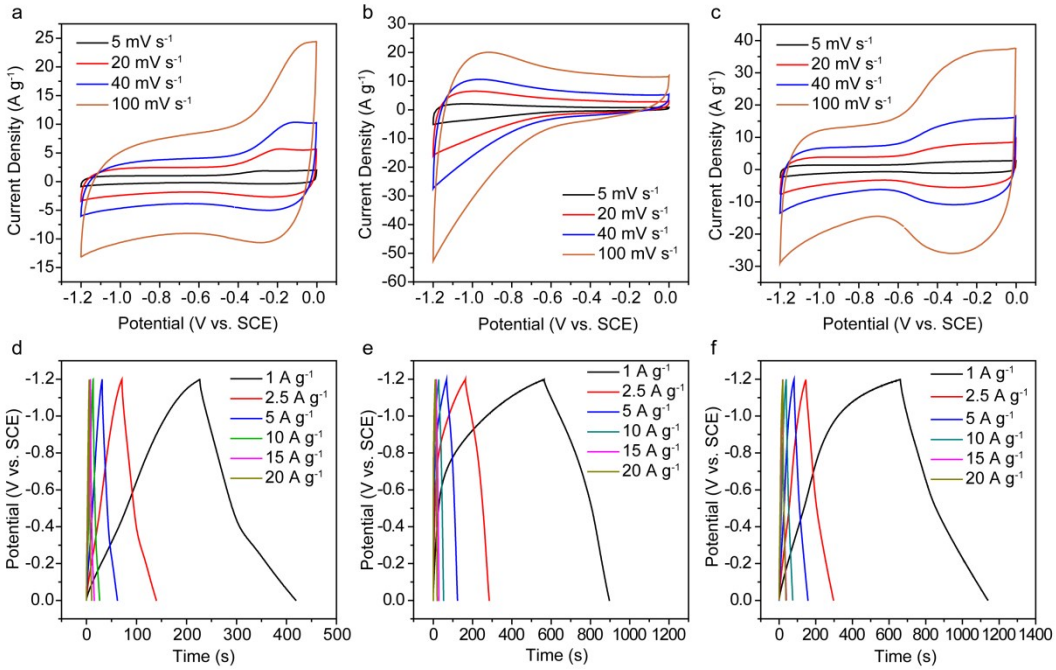

Figure S10. CV curves of (a) PPy, (b) MoO_x and (c) LbL–PPy/MoO_x at different scan rates. Constant current charge–discharge profiles of (d) PPy, (e) MoO_x and (f) LbL–PPy/MoO_x at different current densities.

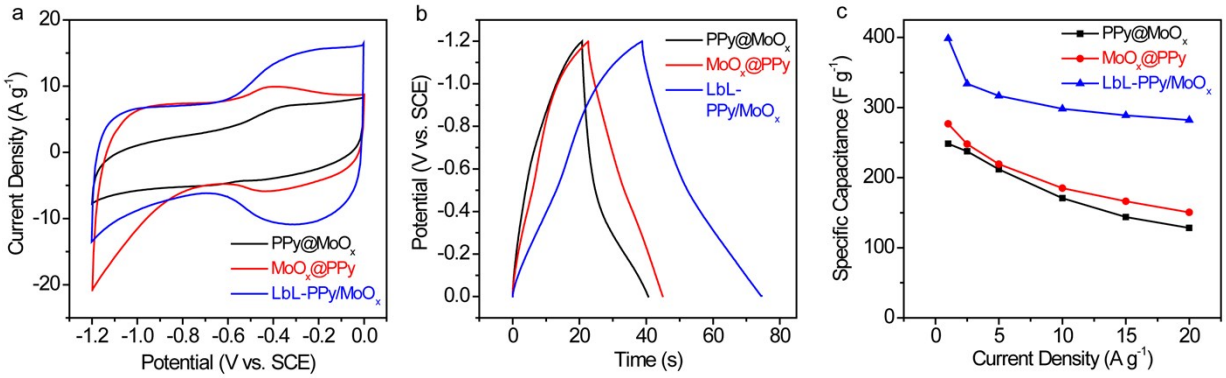

Figure S11. (a) CV curves of PPy@MoO_x, MoO_x@PPy and LbL–PPy/MoO_x at 40 mV s^{-1}. (b) Constant current charge–discharge profiles of PPy@MoO_x, MoO_x@PPy and LbL–PPy/MoO_x at 10 A g^{-1}. (c) Specific capacitance of PPy@MoO_x, MoO_x@PPy and LbL–PPy/MoO_x as a function of current density.

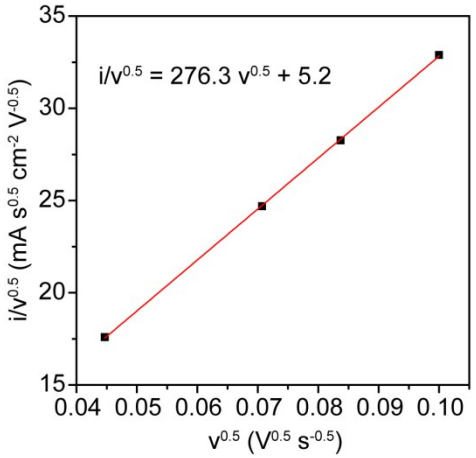

Figure S12. i(V)/$v^{1/2}$ *vs.* $v^{1/2}$ plot collected for LbL–PPy/MoO_x using the anodic current at a selected potential of –0.2 V *vs.* SCE.

Dunn Method: According to Dunn method, the current response at a fixed potential comes from two separate mechanisms, capacitive–controlled and diffusion–controlled processes:

$$i(\mathrm{V}) = k_1 v + k_2 v^{1/2} \quad (15)$$

Where $k_1 v$ stands for the current contributions from the capacitive effects, and $k_2 v^{1/2}$ corresponds to the current contributions from the diffusion–controlled process. Dividing $v^{1/2}$ on both sides of the equation yields:

$$i(\mathrm{V})/v^{1/2} = k_1 v^{1/2} + k_2 \quad (16)$$

By reading the i(V) at a selected potential from CV curves collected at different scan rates followed by plotting i(V)/$v^{1/2}$ *vs.* $v^{1/2}$, in the linear fitting line, k_1 equals the slope and k_2 equals the y–intercept. Figure S12 shows an example of i(V)/$v^{1/2}$ *vs.* $v^{1/2}$ plots collected for LbL–PPy/MoO_x at a fixed potential of –0.2 V *vs.* SCE in the anodic process. Using the k_1 and k_2 obtained above, current contributions from the capacitive effect ($k_1 v$) and diffusion–controlled process ($k_2 v^{1/2}$) at the specific potential are obtained according to Equation (15).

Through conducting the same steps for other potentials, the capacitive/diffusion contribution is shown in Figure 3d.

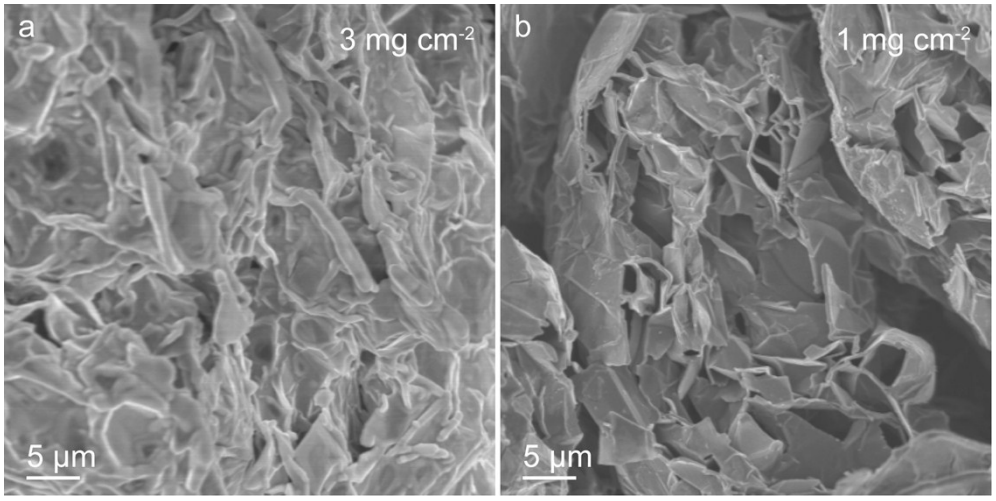

Figure 13. SEM images of LbL–PPy/MoO_x electrodes with mass loading of (a) 3 mg cm^{-2} and (b) 1 mg cm^{-2}.

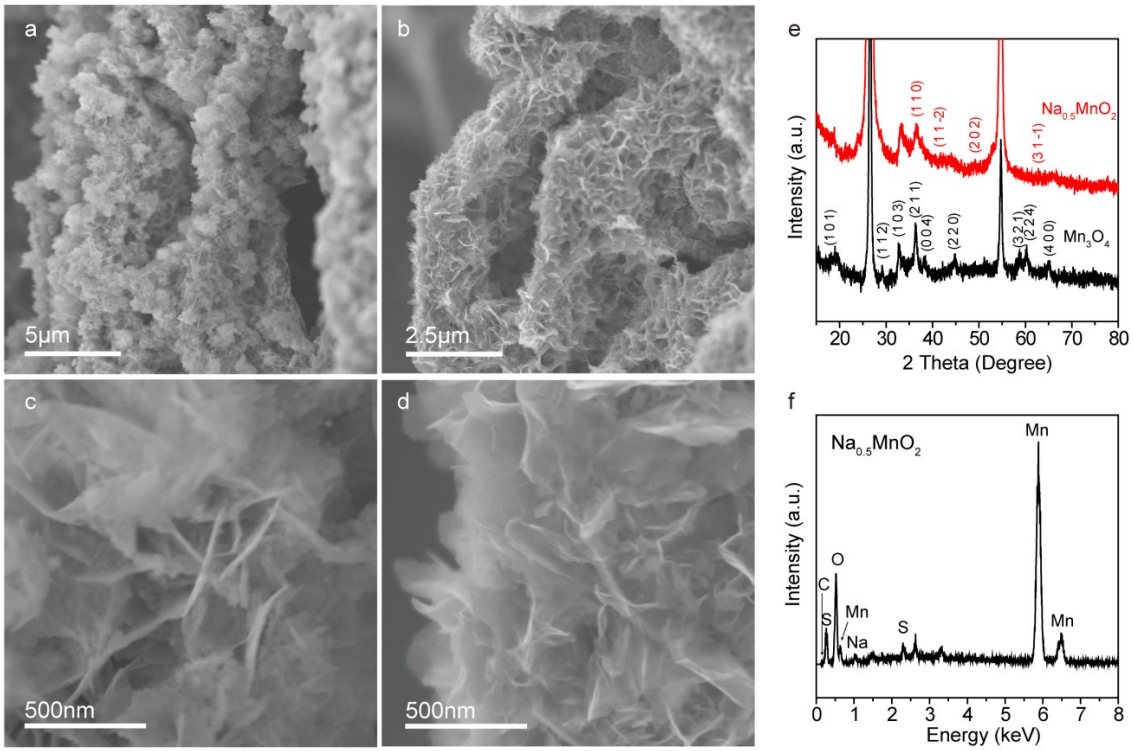

Figure S14. SEM images of (a) Mn_3O_4 and (b) $Na_{0.5}MnO_2$. Magnified SEM images of (c) Mn_3O_4 and (d) $Na_{0.5}MnO_2$. (e) XRD patterns of Mn_3O_4 and $Na_{0.5}MnO_2$. (f) EDS spectra of $Na_{0.5}MnO_2$.

Figure S14a and c show the SEM images of Mn_3O_4 nanoflakes grown on 3D porous EG base. The magnified SEM image reveals the Mn_3O_4 nanoflakes are nearly vertically aligned on the base. After cyclic voltammetry scan, $Na_{0.5}MnO_2$ nanoflakes are obtained (Figure S14b and d). Figure S14e shows

the XRD patterns of the Mn_3O_4 and $Na_{0.5}MnO_2$ materials deposited on EG. For the XRD pattern of Mn_3O_4, except for the diffraction peaks of carbon from EG, all the diffraction peaks can be well indexed to the tetrahedral hausmannite Mn_3O_4 (JCPDS No. 24–0734). After cyclic voltammetry scan, the diffraction peaks of Mn_3O_4 disappear while the new diffraction peaks can be indexed to monoclinic Birnessite (JCPDS No. 43–1456), revealing the phase transition from Mn_3O_4 to $Na_{0.5}MnO_2$. Moreover, Na signal was detected for $Na_{0.5}MnO_2$, which further indicates the transition to $Na_{0.5}MnO_2$. These observations are high consistent with the results reported before.[1]

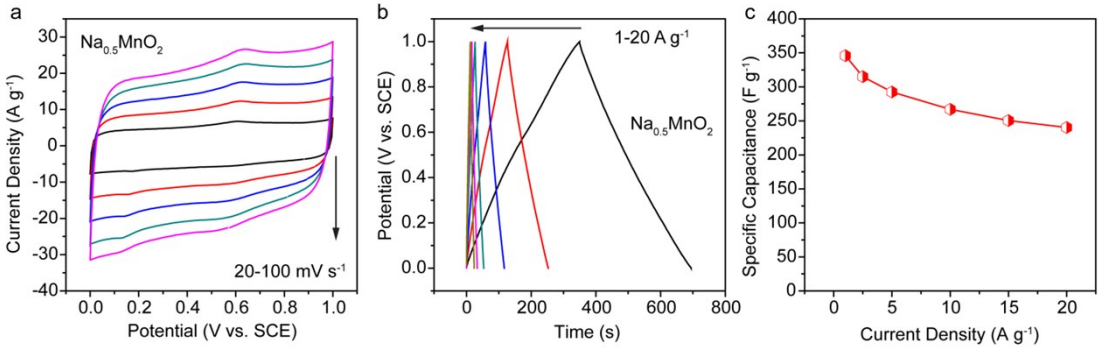

Figure S15. (a) CV curves of $Na_{0.5}MnO_2$ at different scan rates. (b) Constant current charge–discharge profiles of $Na_{0.5}MnO_2$ at different current densities. (c) Specific capacitance of $Na_{0.5}MnO_2$ as a function of current density.

Figure S15a shows the CV curves of $Na_{0.5}MnO_2$ at different scan rates. The shape of CV curves maintains nearly rectangular without distortion even at a scan rate of 100 mV s^{-1}, revealing the ideal capacitive behavior and good rate capability. Constant current charge–discharge profiles of $Na_{0.5}MnO_2$ exhibit an approximately symmetric triangle shapes with negligible *IR* drops, indicating pseudocapacitive behavior and the small resistance of the electrode. Figure S15c shows the specific capacitance of $Na_{0.5}MnO_2$ as a function of current density. The $Na_{0.5}MnO_2$ electrode achieves a good specific capacitance of 346 F g^{-1} at 1 A g^{-1}. At a high current density of 20 A g^{-1}, it can still achieve a high capacitance of 240 F g^{-1}.

Table S1. Specific capacitances of the recently reported negative electrode materials for supercapacitors.

Electrode	*Electrolyte*	*Potential Window (V)*	*Specific Capacitance (maximum)*	*Specific Capacitance (minimum)*
H_xMoO_{3-y}[2]	Sea Water	–0.9~–0.1	250 F g^{-1}@1 A g^{-1}	122 F g^{-1}@20 A g^{-1}
K_yMoO_{3-x}[3]	5 M LiCl	–0.9~–0.1	325 F g^{-1}@0.5 A g^{-1}	186 F g^{-1}@100 A g^{-1}
MoO_{3-x}/CNT[4]	5 M LiCl	–0.9~–0.1	337 F g^{-1}@0.5 A g^{-1}	214 F g^{-1}@10 A g^{-1}
Graphene/MoO_3[5]	1 M Na_2SO_4	–1~0	291 F g^{-1}@2 mV s^{-1}	75 F g^{-1}@50 mV s^{-1}
α–MoO_3[6]	0.5 M Li_2SO_4	–1.0~–0.3	369 F g^{-1}@0.1 A g^{-1}	207 F g^{-1}@1 A g^{-1}
m–MoO_2[7]	1 M LiOH	–1.2~–0.5	146 F g^{-1}@5 mV s^{-1}	69 F g^{-1}@500 mV s^{-1}
MoO_3/PPy[8]	1 M Na_2SO_4	–0.5~0.5	123 F g^{-1}@0.27 A g^{-1}	104 F g^{-1}@2.67 A g^{-1}
SnO_2/PPy[9]	1 M Na_2SO_4	–0.8~0	260 F g^{-1}@1 A g^{-1}	189 F g^{-1}@50 A g^{-1}
V_2O_5@PPy[10]	1 M Na_2SO_4	–0.4~0.5	344 F g^{-1}@0.2 A g^{-1}	189 F g^{-1}@10 A g^{-1}
Fe_2O_3/FGS[11]	1 M Na_2SO_4	–1~0	347 F g^{-1}@10 mV s^{-1}	140 F g^{-1}@1.6 V s^{-1}
H–TiO_2@C[12]	5 M LiCl	–1~0	253 F g^{-1}@10 mV s^{-1}	178 F g^{-1}@400 mV s^{-1}
VN[13]	5 M LiCl	–1.2~0	299 F g^{-1}@10 mV s^{-1}	213 F g^{-1}@100 mV s^{-1}
PPy@V_2O_5[14]	0.5 M K_2SO_4	–0.9~0.1	308 F g^{-1}@0.1 A g^{-1}	Not reported
TiN@C[15]	1 M KOH	–1~0	159 F g^{-1}@0.25 A g^{-1}	125 F g^{-1}@5 A g^{-1}
Fe_2O_3/PPy[16]	1 M Na_2SO_4	–0.8~0	316 F g^{-1}@0.5 mA cm^{-2}	100 F g^{-1}@6 mA cm^{-2}
CNT–rGO[17]	1 M Na_2SO_4	–0.8~0	280 F g^{-1}@1 A g^{-1}	190 F g^{-1}@20 A g^{-1}
Fe_2N[18]	1 M LiCl	–0.8~0	168 F g^{-1}@10 mV s^{-1}	129 F g^{-1}@100 mV s^{-1}
PPy/MoO_x [This work]	**5 M LiCl**	**–1.2~0**	**398 F g^{-1}@1 A g^{-1}**	**282 F g^{-1}@20 A g^{-1}**

Table S2 Energy density and cycling stability of energy storage devices assembled by using PPy or MoO_x as the electrode materials.

Device	***Energy Density***	***Cycling Stability***
MoO_3//MoO_3[19]	22.9 Wh kg^{-1} @ 0.69 kW kg^{-1}	96.5% in 20000 cycles
MoO_3@PPy//$LiMn_2O_4$[20]	45.0 Wh kg^{-1} @ 0.35 kW kg^{-1}	90% in 150 cycles
SnO_2/PPy//SnO_2/MnO_2[9]	27.2 Wh kg^{-1} @ 0.85 kW kg^{-1}	80% in 2000 cycles
MnO_2@PPy//AC[21]	25.8 Wh kg^{-1} @ 0.90 kW kg^{-1}	90.3% in 6000 cycles
CNT@MnO_2//CNT@PPy[22]	40.0 Wh kg^{-1} @ 0.52 kW kg^{-1}	85% in 5000 cycles
$NiMoO_4 \cdot xH_2O$//H_xMoO_3[23]	55.6 Wh kg^{-1} @ 0.64 kW kg^{-1}	81% in 5000 cycles
Graphene/MnO_2//Graphene/MoO_3[5]	42.6 Wh kg^{-1} @ 0.28 kW kg^{-1}	~81.1% in 1000 cycles
PANI//MoO_3[24]	71.9 Wh kg^{-1} @ 0.25 kW kg^{-1}	78% in 1000 cycles
$MgCo_2O_4$@PPy//AC[25]	33.4 Wh kg^{-1} @ 0.32 kW kg^{-1}	91% in 10000 cycles
Co_3O_4@PPy@MnO_2//AC[26]	34.3 Wh kg^{-1} @ 0.08 kW kg^{-1}	100.4% in 11000 cycles
CoO@PPy//AC[27]	43.5 Wh kg^{-1} @ 0.09 kW kg^{-1}	91.5% in 20000 cycles
PPy//PPy[28]	32.9 Wh kg^{-1} @ 0.65 kW kg^{-1}	80.1% in 5000 cycles
PPy@MoO_3//AC[29]	28.0 Wh kg^{-1} @ 0.46 kW kg^{-1}	93% in 1800 cycles
NNA@MnO_2//NNA@PPy[30]	48.9 Wh kg^{-1} @ 1.28 kW kg^{-1}	106.6% in 20000 cycles
LbL–PPy/MoO_x//$Na_{0.5}MnO_2$	**72.7 Wh kg^{-1} @ 0.34 kW kg^{-1}**	**92.3% in 10000 cycles**
This work		

3. REFERENCES

1 N. Jabeen, A. Hussain, Q. Xia, S. Sun, J. Zhu and H. Xia, *Adv. Mater.*, 2017, **29**, 1700804.

2 L. Huang, X. Gao, Q. Dong, Z. Hu, X. Xiao, T. Li, Y. Cheng, B. Yao, J. Wan, D. Ding, Z. Ling, J. Qiu and J. Zhou, *J. Mater. Chem. A*, 2015, **3**, 17217-17223.

3 X. Xiao, C. Zhang, S. Lin, L. Huang, Z. Hu, Y. Cheng, T. Li, W. Qiao, D. Long, Y. Huang, L. Mai, Y. Gogotsi and J. Zhou, *Energy Storage Mater.*, 2015, **1**, 1-8.

4 X. Xiao, Z. Peng, C. Chen, C. Zhang, M. Beidaghi, Z. Yang, N. Wu, Y. Huang, L. Miao, Y. Gogotsi and J. Zhou, *Nano Energy*, 2014, **9**, 355-363.

5 J. Chang, M. Jin, F. Yao, T. H. Kim, V. T. Le, H. Yue, F. Gunes, B. Li, A. Ghosh, S. Xie and Y. H. Lee, *Adv. Funct. Mater.*, 2013, **23**, 5074-5083.

6 J. Jiang, J. Liu, S. Peng, D. Qian, D. Luo, Q. Wang, Z. Tian and Y. Liu, *J. Mater. Chem. A*, 2013, **1**, 2588-2594.

7 X. Li, J. Shao, J. Li, L. Zhang, Q. Qu and H. Zheng, *J. Power Sources*, 2013, **237**, 80-83.

8 X. Zhang, X. Zeng, M. Yang and Y. Qi, *ACS Appl. Mater. Inter.*, 2014, **6**, 1125-1130.

9 F. Grote and Y. Lei, *Nano Energy*, 2014, **10**, 63-70.

10 J. G. Wang, H. Liu, H. Liu, W. Hua and M. Shao, *ACS Appl. Mater. Inter.*, 2018, **10**, 18816-18823.

11 H. Xia, C. Hong, B. Li, B. Zhao, Z. Lin, M. Zheng, S. V. Savilov and S. M. Aldoshin, *Adv. Funct. Mater.*, 2015, **25**, 627-635.

12 X. Lu, M. Yu, G. Wang, T. Zhai, S. Xie, Y. Ling, Y. Tong and Y. Li, *Adv. Mater.*, 2013, **25**, 267-272.

13 X. Lu, M. Yu, T. Zhai, G. Wang, S. Xie, T. Liu, C. Liang, Y. Tong and Y. Li, *Nano Lett.*, 2013, **13**, 2628-2633.

14 Q. Qu, Y. Zhu, X. Gao and Y. Wu, *Adv. Energy Mater.*, 2012, **2**, 950-955.

15 X. Lu, T. Liu, T. Zhai, G. Wang, M. Yu, S. Xie, Y. Ling, C. Liang, Y. Tong and Y. Li, *Adv. Energy Mater.*, 2014, **4**, 1300994.

16 L. Wang, H. Yang, X. Liu, R. Zeng, M. Li, Y. Huang and X. Hu, *Angew. Chem., Int. Ed.*, 2017, **56**, 1105-1110.

17 Z. Zhang, F. Xiao, L. Qian, J. Xiao, S. Wang and Y. Liu, *Adv. Energy Mater.*, 2014, **4**, 1400064.

18 C. Zhu, P. Yang, D. Chao, X. Wang, X. Zhang, S. Chen, B. K. Tay, H. Huang, H. Zhang, W. Mai and H. J. Fan, *Adv. Mater.*, 2015, **27**, 4566-4571.

19 B. Yao, L. Huang, J. Zhang, X. Gao, J. Wu, Y. Cheng, X. Xiao, B. Wang, Y. Li and J. Zhou, *Adv. Mater.*, 2016, **28**, 6353-6358.

20 W. Tang, L. Liu, Y. Zhu, H. Sun, Y. Wu and K. Zhu, *Energy Environ. Sci.*, 2012, **5**, 6909-6913.

21 W. He, C. Wang, F. Zhuge, X. Deng, X. Xu and T. Zhai, *Nano Energy*, 2017, **35**, 242-250.

22 Q. Tang, M. Chen, C. Yang, W. Wang, H. Bao and G. Wang, *ACS Appl. Mater. Inter.*, 2015, **7**, 15303-15313.

23 G. Qu, T. Li, S. Jia, H. Zheng, L. Li, F. Cao, H. Wang, W. Ma, Y. Tang and J. Wang, *Adv. Funct. Mater.*, 2017, **27**, 1700928.

24 H. Peng, G. Ma, J. Mu, K. Sun and Z. Lei, *J. Mater. Chem. A*, 2014, **2**, 10384-10388.

25 H. Gao, X. Wang, G. Wang, C. Hao, S. Zhou and C. Huang, *Nanoscale*, 2018, **10**, 10190-10202.

26 L. Han, P. Tang and L. Zhang, *Nano Energy*, 2014, **7**, 42-51.

27 C. Zhou, Y. Zhang, Y. Li and J. Liu, *Nano Lett.*, 2013, **13**, 2078-2085.

28 Z. H. Huang, Y. Song, X. X. Xu and X. X. Liu, *ACS Appl. Mater. Inter.*, 2015, **7**, 25506-25513.

29 F. Wang, Z. Liu, X. Wang, X. Yuan, X. Wu, Y. Zhu, L. Fu and Y. Wu, *J. Mater. Chem. A*, 2016, **4**, 5115-5123.

30 C. Xu, Z. Li, C. Yang, P. Zou, B. Xie, Z. Lin, Z. Zhang, B. Li, F. Kang and C. P. Wong, *Adv. Mater.*, 2016, **28**, 4105-4110.